

# Guide filter-based gradient vector flow module for infrared image segmentation

FAN ZHAO,<sup>1,2</sup> JIAN ZHAO,<sup>1,\*</sup> WENDA ZHAO,<sup>1,2</sup> AND FENG QU<sup>1</sup>

<sup>1</sup>Changchun Institute of Optics, Fine Mechanics and Physics, Chinese Academy of Sciences, 130033 Changchun, China

<sup>2</sup>University of Chinese Academy of Sciences, 100049 Beijing, China

\*Corresponding author: zhaojian6789@126.com

Received 13 July 2015; revised 12 October 2015; accepted 17 October 2015; posted 20 October 2015 (Doc. ID 245931); published 16 November 2015

Infrared image segmentation is a challenging topic since infrared images are characterized by high noise, low contrast, and weak edges. Active contour models, especially gradient vector flow (GVF), have better segmentation performance for clear images. However, the GVF model has the drawbacks of sensitivity to noise and adaptability of the parameters, decreasing the effect of infrared image segmentation significantly. To address these problems, this paper proposes a guide filter-based gradient vector flow module for infrared image segmentation (GFGVF). First, a guide filter is exploited to construct a novel edge map, providing characteristics of the image edge while excluding the effects of noise. This alleviates the possibility of edge leakage caused by using the traditional edge map. Then, a novel weighting function is constructed to effectively handle the extended capture range and preserving the edge even with noise existing. The experimental results demonstrate that the GFGVF model possesses good properties such as large capture range, concavity convergence, noise robustness, and alleviative boundary leakage. © 2015 Optical Society of America

**OCIS codes:** (100.2960) Image analysis; (100.3008) Image recognition, algorithms and filters; (100.5010) Pattern recognition.

<http://dx.doi.org/10.1364/AO.54.009809>

## 1. INTRODUCTION

Target segmentation is very important in infrared image analysis and target detection. Therefore, the research on effective segmentation of infrared images has attracted many scholars' attention. Although many impressive efforts have been devoted to infrared image segmentation, it remains a challenging problem mainly because of the intrinsic attributes of infrared images. The existing methods [1–6] include morphological operations [1–3], the wavelet transform [4], and the active contour model [5,6].

The active contour model based on curve evolution theory is widely used in image segmentation and has proved to be an effective method. In the segmentation processing, curve evolution is driven by a combination of internal forces and external forces, and it stops on the target boundary of the image by minimizing the energy function. Active contours can also be used in target tracking [7,8] and shape recovery [9].

Typically, active contour models are divided into two categories: parametric active contour models [5,10–12] and geometric active contour models [13–17]. We focus on parametric active contours for infrared image segmentation in this paper. By making some changes, our method can also be extended to geometric active contour models. The energy function is composed of internal forces and external forces. In image

segmentation, the role of an external force is to make the curve move toward the target edge. A lot of work [10,18–25] has been done in constructing the external force, such as balloons [18], distance potential force [19], gradient vector flow (GVF) [10] including its generalization (GGVF) [11] and improvement [20–25]. Among all these external forces, GVF has proved to be the most effective. But there exist some disadvantages such as noise sensitivity and adaptability of parameters, which will be elaborately analyzed in Section 2.B. Although improved methods based on GVF [18–25] have reduced noise sensitivity in some aspects, they cannot be used to handle the featuring noisy boundary points along with noisy edges appropriately. Because the GVF method is based on the gradient of the image, the edge map plays an important role in constructing the external forces; how to obtain the ideal edge map becomes an urgent problem. The guide filter [26], introduced by He in 2013, has good edge-preserving smoothing properties with its behavior near edges. In this paper, the guider filter is exploited in infrared image segmentation.

In light of the above analysis, this paper provides a novel external force based on GVF but better than it. The main contributions consist of the following aspects:

(1) A novel static external force is proposed. It can not only accurately segment the infrared images but also be used for

other types of images such as noisy medical images and visible images.

(2) A novel edge map is constructed by incorporating the guide filter. It can extract the detailed information of the edge from the infrared image with high noise, low contrast, and weak edges. This alleviates the possibility of edge leakage caused by using the traditional edge map.

(3) Choosing appropriate weighting functions is crucial in achieving the goal of extending the capture range while preserving object boundaries. An alternative weighting function is constructed to achieve a precise balance between extending the capture range and preserving the edge.

The remainder of this paper is arranged as follows. In Section 2, we review the classical parametric active contour and discuss the advantages and disadvantages of existing models. The proposed algorithm is introduced in Section 3. In Section 4, some properties of the algorithm are provided. Finally, we conclude this paper in Section 5.

## 2. BACKGROUND

The classic partial differential model for image segmentation is the snake model introduced by Kass [5]. The curve of  $c(q) = [x(q), y(q)]$ ,  $q \in [0, 1]$  evolves to the boundary of the target when the following energy model is minimized:

$$E(c(q)) = \underbrace{\frac{1}{2} \int_0^1 \alpha |c'(q)|^2 + \beta |c''(q)|^2 dq}_{\text{internal energy}} + \underbrace{\int_0^1 E_{\text{ext}}(c(q)) dq}_{\text{external energy}}, \quad (1)$$

where  $\alpha, \beta$  are weighting parameters. The first item is the internal energy, and it is determined by the geometry of the curve itself. This item is used to constrain curve smoothness and tightness. The second item is an external energy term, and it contains the data information of image. So it can induce the evolution of the curve to the target boundary.

### A. Gradient Vector Flow as the External Force Field

There exists an evident drawback of the snake model. The initial curve should be very close to the object border in order to ensure that the curve locates within the capture range of the external force field. An explanation of this phenomenon is that an external force field based on the gradient can exist only in the region close to the object boundary. Xu and Prince proposed

GVF [10] as the external force field, which largely improved the deficiencies of the snake model. The gradient vector flow, defined as  $V(x, y) = [u(x, y), v(x, y)]$ , can be obtained from the following dynamic evolution equation:

$$V_t(x, y, t) = \mu \nabla^2 V(x, y, t) - |\nabla f|^2 [V(x, y, t) - \nabla f], \quad (2)$$

where  $V_t(x, y, t)$  is the partial derivative of  $V(x, y, t)$ ,  $\nabla^2$  is the Laplace operator expressed as  $\nabla^2 = \partial^2/\partial x^2 + \partial^2/\partial y^2$ ,  $\mu$  is a coefficient to control the smoothness of GVF external force field,  $f$  is the edge map related to the input image of  $I(x, y)$ , and  $\nabla f$  is the gradient of the edge map  $f$ . The parameter  $\mu$  is used to adjust the weight of the first item, and its value is determined by the smoothness of the image. Particular advantages of the GVF snake over the traditional snake are that it expands the capture range of the initial curve, and it possesses the ability of capturing the regions of very high curvature.

### B. Analysis of GVF Active Contour Model

Although the GVF active contour model has some desired conditions, there also exist some drawbacks.

(a) Noise sensitivity:  $f$  is typically defined as the edge map of the image. Figure 1(a) is a reconstructed image curve with doping noise. The edge map  $f$  featuring noisy boundary points along with noisy edges is shown in Fig. 1(c). Even when the initial curve is close to the border of target, it cannot converge correctly. This example demonstrates that due to the use of the edge map information, the GVF method is sensitive to the noise.

As mentioned above, the edge map is a crucial factor in image segmentation. Cheng and Foo [20] proposed a dynamic directional GVF (DDGVF) algorithm by using the gradient directional information for calculating the edge map. Tang [21] extended the DDGVF flow to a multidirectional GVF by computing the directional gradient for each pixel with a varying direction. Kovacs and Sziranyi [22] proposed a Harris based GVF (HGVF) algorithm by using a new feature map. Our effort aims to provide an ideal edge map which can characterize the edge information and is not corrupted by noise.

(b) Lack of adaptability of  $\mu$ : Another drawback of the GVF module is that the weighted parameter  $\mu$  is a constant determined by the noise in the image. Its value is proportional to the size of the noise. However, if  $\mu$  takes an inappropriate value, such as being too large, the evolution curve will pass through the weaker edge and cause erroneous segmentation results. In contrast, if  $\mu$  is too small, the obtained external force field will preserve excessive noise. Xu and Prince [11] introduced the generalized GGVF active contour model to overcome the drawback of the original GVF. In their method, the constant

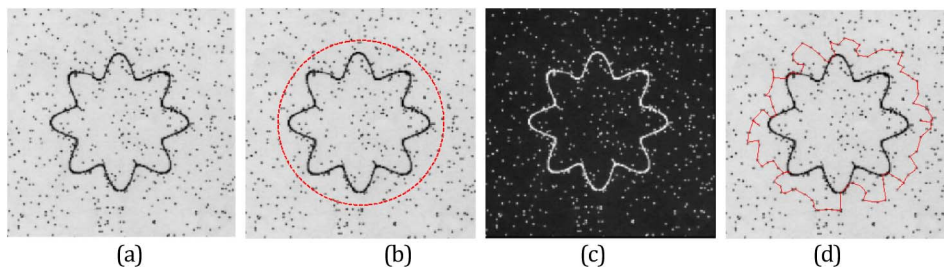


**Fig. 1.** (a) Image with noise, (b) location of the initial curve, (c) edge map of (a), and (d) segment result.

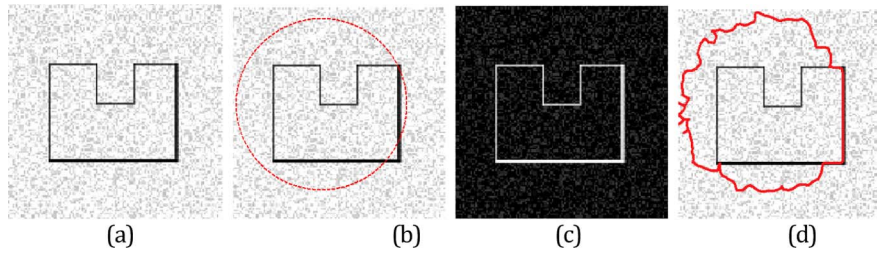


**Fig. 2.** (a) Image with noise, (b) location of the initial curve, (c) edge map of (a), and (d) segment result.

weighting coefficients are replaced by two spatially varying weighting function related to the edge map. However, the relationship between the extended capture ranges and the preserved edges cannot be well handled when there exists noise in the image. The capture range of GVF or GGVF is determined by the smoothness parameter. The larger the smoothness parameter, the greater the capture range is. To achieve accurate segmentation in different images, different values of the smoothness parameter have to be taken. If an improper value is chosen, the segmentation results will be unsatisfactory. As shown in Fig. 2(a), we construct a noisy image to validate the GGVF active contour model in noisy image segmentation. The weighting function related to the smoothness parameter is determined by the edge map, which is damaged by the noise as shown in Fig. 2(c). The initial curve is defined as shown in Fig. 2(b), with the left of the initial curve located farther away from the target boundary, and the right of the initial curve located closer to the target boundary. It can be seen from Fig. 2(d) that the curve closer to the edge of the target could almost stop on the target boundary. However, the curve stops in the error region when it is far away from the target edge. This illustrates that the GGVF active contour model does not have a large capture range in the case of noisy images. Our effort is to construct a new alternative weighting function to overcome the above problems and to ensure the capture range of our algorithm in dealing with the infrared image.

### 3. PROPOSED ALGORITHM

#### A. Novel Edge Map

The calculation of the external force can be divided into two independent steps: the construction of the edge map and the computation of the external force. As mentioned in Section 2, the original edge map is more easily affected by noise, and this brings some disadvantages in the infrared image segmentation. Since the quality of the edge map is a critical factor in snake performance, it is urgent to obtain a desirable edge map. In this section, we propose a new edge map to guide the curve evolution. The new edge map is defined as

$$e(x, y) = \nabla |W_{xy} \times P(x, y)|, \quad (3)$$

where  $\nabla$  is the gradient operator,  $P(x, y)$  is the input image, and  $W_{xy}$  represents the ideal kernel weight. The common method is to define  $W_{xy} = G_{\sigma}(x, y)$ , and  $G_{\sigma}(x, y)$  is the Gaussian kernel. From Fig. 3(b), it can be clearly seen that a blurred edge occurs when using the Gaussian kernel to make convolution with the input image, despite the fact that noise can be removed to a certain extent. In the infrared image segmentation, this will increase the negative impact brought about by the weak edge

and incurs boundary leakage, which is shown in Fig. 3(c). A bilateral filter, proposed in [27], is effective in filtering out noise. If  $W_{xy}$  takes the bilateral filter kernel, the segmentation result is listed in Fig. 3. By observing Fig. 3(d), the noise in the image is removed after bilateral filtering. However, this also introduces gradient reversal artifacts in the boundary, which are detailed in Section 3.A.2. In the segmentation process, the curve does not stop precisely at the edge of the target.

#### 1. Guide Filter

An ideal image edge map should not only provide the distribution of interesting feature but also weaken the impact of the small-scale texture information and noise. However, it is a dilemma to suppress noise and preserve weak edges simultaneously. To overcome the inconvenience brought by the edge map, this paper adopts the guide filter mentioned in [26] to get an ideal edge map.

The model is defined as

$$q_i = a_k I_i + b_k, \quad i \in w_k, \quad (4)$$

where  $a_k$  and  $b_k$  are the coefficients in the window  $w_k$  centered at the pixel  $k$ . In Eq. (4), a predetermined image  $I$  and the input image  $p$  are used to determine the required output image  $q$ . From Eq. (4), we can obtain  $\nabla q = \nabla I$ , and this guarantees that  $q$  has an edge only if  $I$  has an edge. The output image can also be modeled as

$$q_i = p_i + n_i, \quad (5)$$

where  $n_i$  represents the undesired components such as noise or intensity inhomogeneity. To minimize the difference between output image  $q$  and input image  $p$ , we minimize the following function, combining Eq. (4) with Eq. (5):

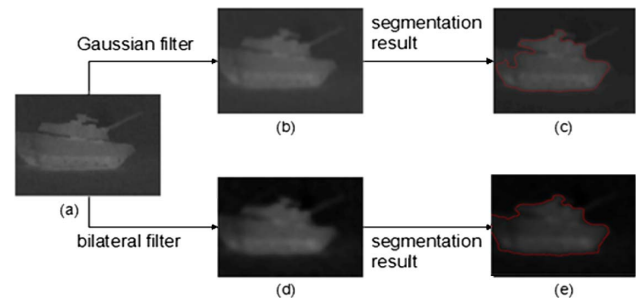


**Fig. 3.** (a) Original infrared image, (b) image after Gaussian filter, (c) segment result, (d) image after bilateral filter, and (e) segment result.

$$E(a_k, b_k) = \sum_{i \in w_k} ((a_k I_i + b_k - p_i)^2 + \lambda a_k^2), \quad (6)$$

where  $\lambda$  is a variance adjustment parameter used to prevent the value of  $a_k$  from being too large. By solving the linear regression equation (6), we have

$$a_k = \frac{\frac{1}{|w|} \sum_{i \in w_k} I_i p_i - \mu_k \bar{p}_k}{\sigma_k^2 + \lambda}, \quad (7)$$

$$b_k = \bar{p}_k - a_k \mu_k, \quad (8)$$

where  $\mu_k$  and  $\sigma_k^2$  are the mean and variance of  $I$  in the window  $w_k$ , respectively, and  $|w|$  is the number of pixels in  $w_k$ .  $\bar{p}_k$  is the mean of all pixels in  $w_k$ , expressed as  $\bar{p}_k = \frac{1}{|w|} \sum_{i \in w_k} p_i$ . The value of  $q_i$  in function (4) is not identical when it is computed in different windows; the average method can be used to strike the value of the output image. After obtaining the coefficients of  $a_k$  and  $b_k$ , the output filtering image can be computed by

$$q_i = \frac{1}{|w|} \sum_{k|i \in w_k} (a_k I_i + b_k) = \bar{a}_i I_i + \bar{b}_i. \quad (9)$$

Here,  $\bar{a}_i = \frac{1}{|w|} \sum_{i \in w_k} a_i$  and  $\bar{b}_i = \frac{1}{|w|} \sum_{i \in w_k} b_i$  are the average coefficients of all windows overlapping pixel  $i$ . According to the revised Eq. (9), the coefficients  $(\bar{a}_i, \bar{b}_i)$  vary spatially, which causes  $\nabla q$  being no longer scale with  $\nabla I$ . Since  $(\bar{a}_i, \bar{b}_i)$  are the average coefficients, their gradients can be expected to be much smaller than that of  $I$  near strong edges. In this situation we can have  $\nabla q \approx \bar{a} \nabla I$ . This means the abrupt change of the intensity in  $I$  will be almost unchanged in the output image of  $q$ . From functions (7) and (8), we can see that  $a_k$  and  $b_k$  can be written as the weighted average of  $p$ , expressed as

$$a_k = \sum_j A_{kj}(I) p_j, \quad (10)$$

$$b_k = \sum_j B_{kj}(I) p_j. \quad (11)$$

$q_k = \sum_j W_{kj}(I) p_j$  can be obtained from formula (11), and the filtering kernel weight is explicitly expressed as

$$W_{ij}(I) = \frac{1}{|w|^2} \sum_{k:(i,j) \in w_k} 1 + \frac{(I_i - \mu_k)(I_j - \mu_k)}{\sigma^2 + \lambda}. \quad (12)$$

## 2. Guide Filter-based Edge Map

In this section, we introduce the novel edge map to overcome the above-mentioned drawback of GVF and GGVF. Let the novel edge map be expressed as

$$e(x, y) = \nabla |W_{xy}(I(x, y)) \times P(x, y)|. \quad (13)$$

$P(x, y)$  represents the input image, and  $I(x, y)$  is the guided image. In order to obtain satisfactory filtering results, the guidance  $I(x, y)$  is identical to the input  $P(x, y)$  in our method by referring to [26]. Figure 4 shows the comparison of edge maps obtained from different approaches. In Fig. 4(c), the gradient edge map of the original image is affected by noise and cannot provide effective image data for guiding curve evolution. We can see from Fig. 4(d) that the brightness unevenness in the local region and the noise are removed to a great extent.

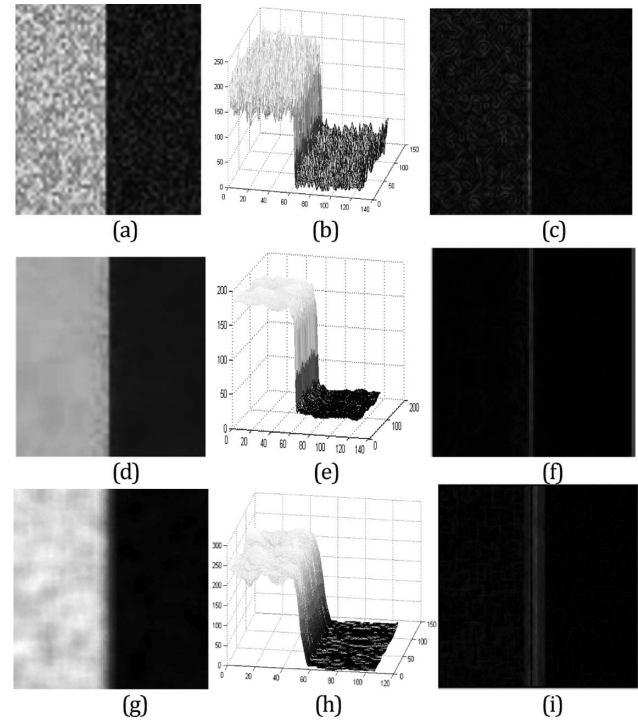


**Fig. 4.** (a) Original image with greater noise, (b) three-dimensional gray-scale image corresponding to (a), (c) edge map of (a), (d) guide filtered image, (e) three-dimensional gray-scale image of (d), (f) new edge map of (d), (g) bilateral filtered image, (h) three-dimensional gray-scale image of (g), and (i) new edge map of (g).

Figure 4(e) provides the filtered effect in a more intuitive way. More importantly, the edge map of the image obtained from function (13) is well retained and barely weakened as shown in Fig. 4(f), which is always critical in the segmentation of an infrared image containing a weak edge. By using the proposed edge map, we can eliminate the false boundary caused by the noise and preserve the weak edge well. This is critical in the method based on the GVF, which is analyzed in Section 2.B, because the edge map plays a guiding role in the process of curve evolution. The guide filter-based edge map can provide the edge information of the infrared image and avoid being affected by noise. This avoids the incorrect segmentation results caused by noise and oversegmentation due to the weak edge. If a bilateral filter is used as shown in Figs. 4(g)–4(i), the edge of the image is destroyed even if the noise is removed. As Fig. 4(i) illustrates, there exist gradient reversal artifacts near the edge which cause inaccurate or erroneous segmentation.

## B. Weighting Function-based Energy Function

The external field is defined as a vector field  $V(x, y) = [u(x, y), v(x, y)]$  by minimizing the following energy function:

$$E(V) = \iint g(x, y) \times |\nabla V|^2 dx dy + b(x, y) \times |V - \nabla e|^2 dx dy, \quad (14)$$

where  $g(x, y)$  and  $b(x, y)$  are the weighted functions. The first item, working in the homogenization region away from edge regions, has an isotropic smoothing effect on the fields and

is called a smoothing energy item. The second item, working in the edge region, is called an edge energy item, forcing the vector field  $V(x, y) = \nabla e$ . The first term guarantees the curve has an extended capture range, and the second term preserves the edge of the object. So it is crucial to select the appropriate weighting functions. The weighting function is defined as follows:

$$g(x, y) = \phi(e)b(x, y) = 1 - g(x, y), \quad (15)$$

where  $\phi(e)$  is the function related to the edge map  $e$ . In the homogeneous regions, we hope  $g(x, y) = 1$  and  $b(x, y) = 0$ , so the first smoothing item will play a main role and the vector field will be slowly varying (or smooth) at locations far from the edges. In the edge regions, we desire  $g(x, y) = 0$  and  $b(x, y) = 1$ . In this way, the smoothing term almost does no work, avoiding a smoothing effect on the edge. Meanwhile, the second term plays a major role, achieving the goal of preserving the edge of the target. In the regions between edge and homogeneous regions, called transition regions, the values of  $g(x, y)$  and  $b(x, y)$  are changed between 0 and 1, which induces the vector field to continuously extend from the edge regions to the homogeneous regions. Overall, by selecting the appropriate weighting coefficients, the method could extend the capture ranges while preserving edges.

Because the weighting function is related to the edge map, it is crucial to provide good edge localization unaffected by some unfavorable factors such as noise. Therefore, the weighting function is defined to be relevant with the novel edge map of  $e$ . There many ways to define the weight function, and in this paper the function is expressed as

$$b(x, y) = \begin{cases} 1, & |e| \geq \tau \\ -\frac{e^3}{8\tau^3} + \frac{5e}{8\tau} + \frac{1}{2}, & 0 < |e| < \tau \\ 0, & |e| = 0 \end{cases}$$

$$g(x, y) = 1 - b(x, y), \quad (16)$$

In Eq. (16), the edge function  $e$  is normalized to the range from 0 to 1, and  $\tau$  is a positive number. Our weight function is different from GGVF, whose weight function is related to the gradient of the edge map, and the proposed function is based on the edge map itself.

### C. Numerical Implementation

Now, the vector field can be acquired by minimizing Eq. (14). According to the variable differential method, the Euler–Lagrange functional of the energy function  $E(V)$  is expressed as

$$g\nabla^2 V - b(V - \nabla e) = 0. \quad (17)$$

In order to obtain the vector field  $V$  in Eq. (17), we introduce a virtual variable  $t$  and establish the following partial differential equation (PDE):

$$\frac{\partial V}{\partial t} = g\nabla^2 V - b(V - \nabla e). \quad (18)$$

The above function can be solved by finding the equilibrium solution of the following PDEs:

$$\begin{cases} u_t = g\nabla^2 u - b(u - e_x), & e_x = \frac{\partial e}{\partial x} \\ v_t = g\nabla^2 v - b(v - e_y), & e_y = \frac{\partial e}{\partial y} \end{cases} \quad (19)$$

By using the finite difference scheme to iterate the above PDEs, the numerical solution of function (18) can be written as

$$\begin{aligned} V(x, y, t + \Delta t) = & (1 - b\Delta t)V(x, y, t) + r[V(x + 1, y, t) \\ & + [V(x - 1, y, t)] + [V(x, y + 1, t)] \\ & + [V(x, y - 1, t)] - 4[V(x, y, t)]] + \Delta t c \end{aligned} \quad (20)$$

By making  $\begin{cases} b = b \\ c = b\nabla e \end{cases}$ , Eq. (20) can be expressed as

$$\begin{aligned} V(x, y, t + \Delta t) = & (1 - b\Delta t)V(x, y, t) + r[V(x + 1, y, t) \\ & + [V(x - 1, y, t)] + [V(x, y + 1, t)] \\ & + [V(x, y - 1, t)] - 4[V(x, y, t)]] + \Delta t b\nabla e. \end{aligned} \quad (21)$$

In order to ensure the stability of the iterative algorithm, we need to define a finite difference grid ratio as  $r = \frac{g\nabla e}{\Delta x^2} \leq \frac{1}{4}$ .

The computational complexity of the proposed active contour is mainly determined by two factors: the computation of the external force field and the front propagation of the active contour. Both the generation of the external force field and the propagation of the contour front are iterative processes. Unlike the GGVF model, in the iterative processes, the edge map is constructed with the guide filter kernel function instead of the Gaussian kernel. In calculating the guide filter kernel function, five addition/subtraction operations and one division operation are utilized per pixel, and the computational complexity of the novel edge map is  $O(N)$ , whereas the computational complexity of the edge map by using a Gaussian filter is  $O(N^2)$  and  $O(N^2) > O(N)$ . Meanwhile, in calculation of the weighting function, the new edge function is used directly in our method. Compared to GGVF, which uses the gradient of the edge map to construct the weighting function, our approach reduces the computational complexity to a great extent.

## 4. RESULTS AND ANALYSIS

In order to better filter out noise and retain the weak edge of the image, it is important to select the appropriate window parameter  $|w|$  and variance adjustment parameter  $\lambda$  in function (12). In the homogeneous area, the filter results are better with a larger window parameter  $|w|$ . In heterogeneous areas, a larger window brings unfavorable filter results. Simultaneously,  $\lambda$  is a regularization parameter penalizing large  $a_k$ . The local areas with variance  $\sigma_k^2$  much smaller than  $\lambda$  are smoothed, whereas those with variance much larger than  $\lambda$  are preserved. It determines whether the local area is an edge or a high variance patch that should be preserved. It is necessary to choose a reasonable  $|w|$  and  $\lambda$ . In order to filter noise and retain the edge of an infrared image, we choose  $|w| = 4$  and  $\lambda = 0.04$  in this paper. The specification of  $\tau$  determines, to some extent, the degree of trade-off between field smoothness and gradient conformity, which is set to 0.1 in all of our experiments.

To demonstrate the effectiveness of the algorithm, we list a few properties of the proposed algorithm. The GVF field is an external force derived from the image edge, but it has a larger scope compared with the traditional snake module. The scope of the GVF field is not limited to the image edge adjacent area,

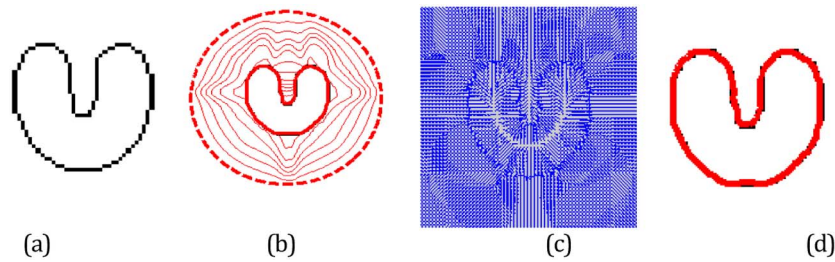


**Fig. 5.** (a) U-shape image, (b) evolution of the curve, (c) force field of (a), and (d) segment result.

and it can capture the entire area of the image. For this reason, we will compare our algorithm with the GVF snake module and some improved algorithms based on GVF.

### A. Capture Range, Convergence to Concavity, and Initialization Insensitivity

In the experiments, the U-shape image is used to prove the effectiveness of our algorithm. The contour line of our proposed model moves from a farther position to the target boundary; the movement process is shown in Fig. 5(b). Finally, the contour line succeeds in fitting object boundaries, which proves that the proposed method has the property of concavity convergence. As shown in Fig. 5(c), the effective force field of our model is distributed throughout the image area. In order to test and verify the initialization sensitivity of our algorithm, the initial

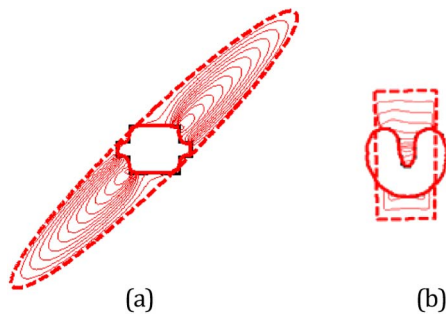


**Fig. 6.** (a) Evolution of curve and (b) evolution of curve.

curves are placed at different positions as shown in Figs. 6(a) and 6(b). Even if the position of the initial curve keeps away from the target boundary or crosses through the target boundary, our model can obtain accurate segmentation results.

### B. Preventing Weak Edge Leakage

Figure 7 illustrates the effectiveness of the modified edge map for image segmentation. Figure 7(a) is an infrared image. In this part, we use it for weak edge leakage analysis. In calculating the feature map, the HGVF active contour model uses a Gaussian convolution to avoid the influence of noise on the segmentation processing, and typically the boundary noise is filtered. As mentioned in Section 3.A, this method weakens the weak edges as well, making it more difficult to segment exactly. Figures 7(c)–7(e) clearly illustrate this phenomenon. Because the weak edge is weakened further, which is detrimental to the segmentation processing, the infrared image segment result appears with weak edge leakage as shown in Fig. 7(d). By adopting our method, the edge of the image can almost be preserved while noise is filtered out, as shown in Fig. 7(c). In the process of segmentation, the calculation of external force and the evolution of the curve are both related to the edge map. An ideal edge map without noise and weakened object boundaries is helpful to accurately obtain the segmentation result. We can observe from Fig. 7(g) that the guide filter-based edge map can characterize the boundary property of Fig. 7(a) without noise. Under such conditions, the weighting function is not affected by the noise and also avoids the boundary leakage caused by the weak edge as shown in Figs. 7(h) and 7(i).

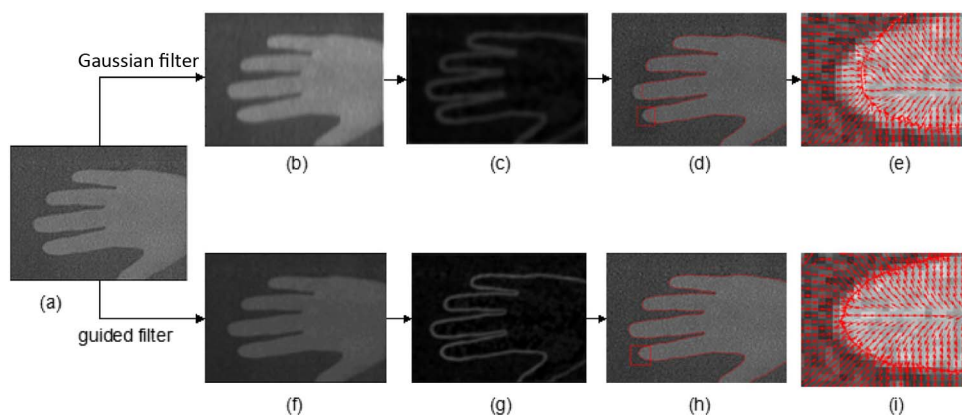


**Fig. 7.** (a) Original image with weak edge and containing noise, (b) image after Gaussian filter, (c) Gaussian filter-based edge map, (d) HGVF result with  $\lambda = 0.1$  and  $\rho = 0.01$ , (e) partial vector field of (d), (f) image after guide filter, (g) guide filter-based edge map, (h) proposed method, and (i) partial vector field of (h).

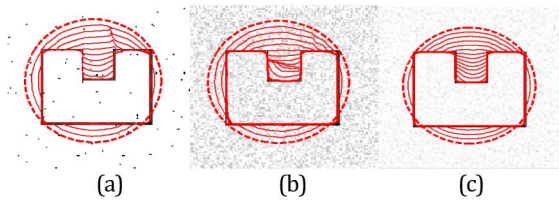


**Fig. 8.** (a) Image with salt-and-pepper noise, (b) image with speckle noise, and (c) image with Gaussian noise.

### C. Noise Sensitivity

In order to test the noise sensitivity of the proposed algorithm, different types of noises are added to the U-shaped image as shown in Figs. 8(a)–8(c). The boundaries of the images are corrupted by noise, and the edge map obtained from the original image gradients are also affected by the noise. By using the proposed edge map, the adverse impact of noise on boundary and smoothness parameters can be avoided. From Fig. 8, we observe that the evolution curve can stop on the target boundary without being affected by noise. In order to prove the robustness of our algorithm further, we enumerate another experimental result.

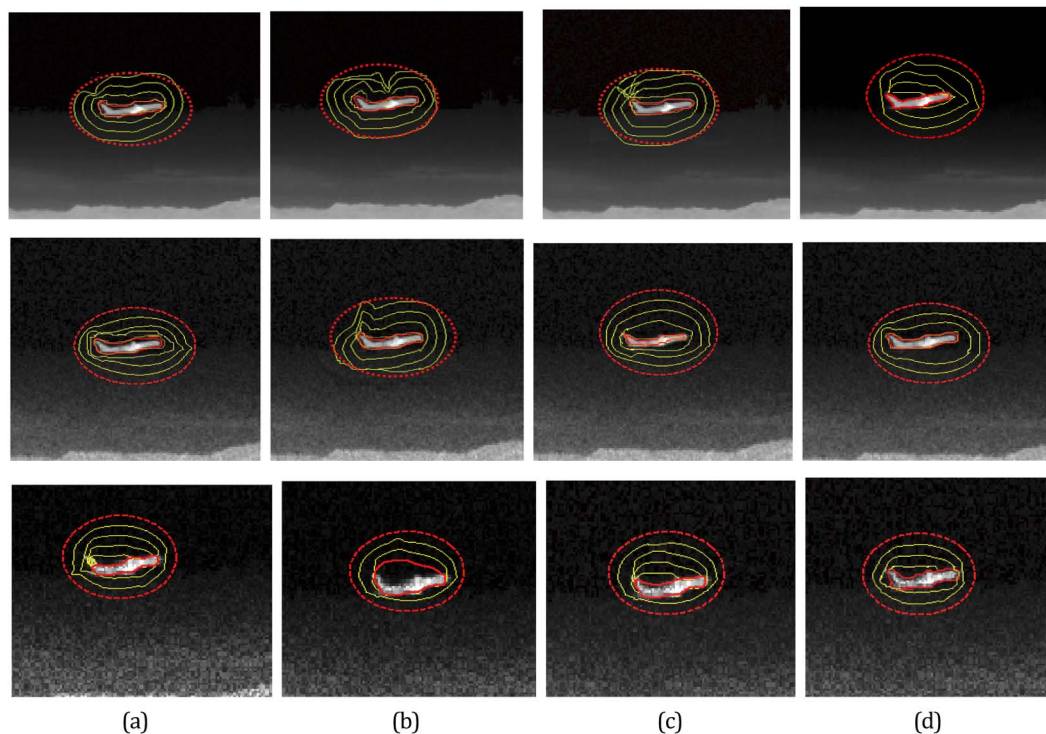
Figures 9(a)–9(d) list the segmentation results of an infrared aircraft image at different noise levels. It can be seen from the first line of Fig. 9 that the evolution curves can converge on the aircraft boundary for all cases when the image contains a lower percentage of noise, with a higher segmentation accuracy acquired by our algorithm. When the proportion of the noise contained in the image increases, as shown in the second line of Fig. 9, the segmentation accuracy is reduced using the normal direction gradient vector flow (NGVF) method. This is

because the NGVF active contour model only adopts the normal direction of diffusion, which cannot stop at weak edges. By using NGVF, the evolution curve passes through the weak edge and converges inside the target. As the noise increases to some extent (as shown in the third line of Fig. 9), GGVF, DDGVF, and NDVF active contour models have erroneous segmentation results. From Fig. 9, we verify that the proposed algorithm is superior to other methods for the segmentation of noisy infrared images.

We demonstrate the above procedure by the following experiment shown in Fig. 10. Figures 10(a)–10(d) show other segmentation results of the infrared images with large noise by different active contour models. It is clear to see the difference of segmentation results of these four modules as dealing with the target edge corrupted by noise. In the edge map calculation process, GGVF uses a Gaussian kernel to make convolution with the edge gradient, which weakens the edge. This is detrimental, causing oversegmentation or erroneous splitting. Both of NGVF and DDGVF modules do not work in the case of a noisy boundary, leading to an erroneous result. The segmentation result of our method as shown in Fig. 10(d) is obviously more accurate than that of the GGVF, DDGVF, and NGVF. The time consumption of different algorithms when dealing with Fig. 9 and Fig. 10 are listed in Table 1.

### D. Segmentation of Other Types of Image

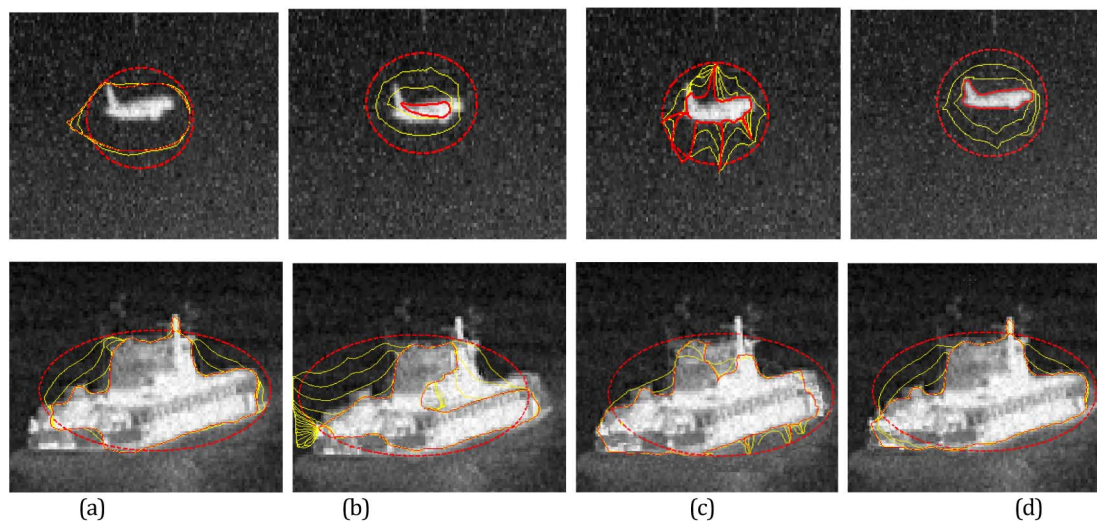
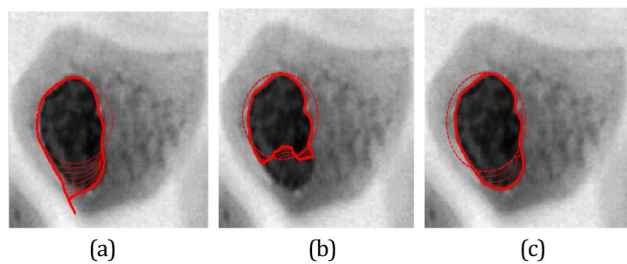
In order to verify the robustness of our algorithm, we segment other types of image not limited to the infrared images. Figure 11 is a medical image with noise, uneven gray distribution, and weak edges. Both of the GGVF and NGVF create erroneous segmentation results. From Fig. 11(c), we observe that the proposed algorithm can effectively deal with such



**Fig. 9.** (a) GGVF, (b) DDGVF with  $\mu = 0.1$  and  $\sigma = 1$ , (c) NGVF with  $\mu = 0.1$ , and (d) proposed method.

**Table 1. Time Consumption of Different Algorithms**

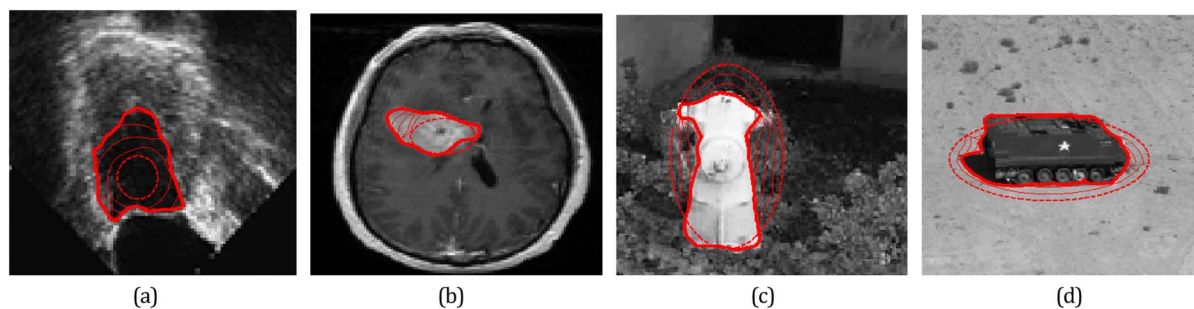
| Image          | Size      | GGVF    | DDGVF    | NGVF    | Proposed Method |
|----------------|-----------|---------|----------|---------|-----------------|
| Fig. 9 line 1  | 220 × 120 | 1.890 s | 2.850 s  | 1.159 s | 1.402 s         |
| Fig. 9 line 2  | 220 × 120 | 1.786 s | 2.518 s  | 1.093 s | 1.512 s         |
| Fig. 9 line 3  | 220 × 120 | 1.760 s | 1.742 s  | 1.569 s | 1.720 s         |
| Fig. 10 line 1 | 256 × 256 | 4.195 s | 3.034 s  | 3.054 s | 2.916 s         |
| Fig. 10 line 2 | 320 × 320 | 9.648 s | 12.752 s | 6.432 s | 7.146 s         |

**Fig. 10.** (a) GGVF, (b) DDGVF with  $\mu = 0.1$  and  $\sigma = 1$ , (c) NGVF with  $\mu = 0.1$ , and (d) proposed method.**Fig. 11.** (a) GGVF, (b) NGVF, and (c) proposed method.

medical images and get satisfactory results. In Fig. 12, other types of images are chosen to exemplify the effectiveness of our active contour model.

## 5. CONCLUSION

In this paper, a guide filter-based GVF module for infrared image segmentation has been introduced. By incorporating the guide filter, a novel edge map is constructed to extract the detailed information of the edge from the infrared image with high noise, low contrast, and weak edges. In addition, we re-defined the weighting function. It can effectively handle the relationship between the extended capture range and preserved edge when noise exists. Through the experimental section, several promising properties of our algorithm have been

**Fig. 12.** More results using the proposed method.

demonstrated, such as large capture range, concavity convergence, and noise robustness. The proposed algorithm can detect and preserve the locations of edges precisely, avoiding noise interference. It can not only accurately segment the infrared images but also be easily adapted to other types of images.

**Funding.** National Natural Science Foundation of China (NSFC) 61137001; National Science and Technology Major Project 2013ZX04007021.

## REFERENCES

- H. Lu, L. Zhang, M. Zhang, X. Hu, and S. Serikawa, "A method for infrared image segment based on sharp frequency localized contourlet transform and morphology," in *International Conference on Intelligent Control and Information Processing* (IEEE, 2010), pp. 79–82.
- S. Krishnamurthy, S. S. Iyengar, R. J. Holyer, and M. Lybanon, "Histogram-based morphological edge detector," *IEEE Geosci. Remote Sens. Lett.* **32**, 759–767 (1994).
- W. Sun and L. Z. Xia, "Infrared target segmentation algorithm based on morphological method," *Int. J. Infrared Millim. Waves* **23**, 233–236 (2004).
- Y. Q. Sun, J. W. Tian, and J. Liu, "Background suppression based on wavelet transformation to detect infrared target," in *Proceedings of 2005 International Conference on Machine Learning and Cybernetics* (IEEE, 2005), pp. 4611–4615.
- M. Kass, A. Witkin, and D. Terzopoulos, "Snakes: active contour models," *Int. J. Comput. Vis.* **1**, 321–331 (1988).
- P. Thourel and C. Collet, "Active contour models for infrared cloudy shapes segmentation," in *Oceans Engineering for Today's Technology and Tomorrow's Preservation* (IEEE, 1994), pp. 444–448.
- N. Paragios and R. Deriche, "Geodesic active regions and level set methods for motion estimation and tracking," *Comput. Vis. Image Underst.* **97**, 259–282 (2005).
- T. Zhang and D. Freedman, "Tracking objects using density matching and shape priors," in *Proceedings of the Ninth IEEE International Conference on Computer Vision* (2008), pp. 1056–1062.
- A. Jalba, M. Wilkinson, and J. Roerdink, "CPM: a deformable model for shape recovery and segmentation based on charged particles," *IEEE Trans. Pattern Anal. Mach. Intell.* **26**, 1320–1335 (2004).
- C. Xu and J. Prince, "Snakes, shapes, and gradient vector flow," *IEEE Trans. Image Process.* **7**, 359–369 (1998).
- C. Xu and J. Prince, "Generalized gradient vector flow external forces for active contours," *Signal Process.* **71**, 131–139 (1998).
- N. Ray and S. Acton, "Motion gradient vector flow: an external force for tracking rolling leukocytes with shape and size constrained active contours," *IEEE Trans. Med. Imag.* **23**, 1466–1478 (2004).
- V. Caselles, R. Kimmel, and G. Sapiro, "Geodesic active contours," *Int. J. Comput. Vis.* **22**, 61–79 (1997).
- M. F. Santarelli, V. Positano, C. Michelassi, M. Lombardi, and L. Landini, "Automated cardiac MR image segmentation: theory and measurement valuation," *Medical Engineering and Physics* **25**, 149–159 (2003).
- D. Nguyen, K. Masterson, and J. P. Valle, "Comparative evaluation of active contour model extensions for automated cardiac MR image segmentation by regional error assessment," *Magn. Reson. Mater. Phys., Biol. Med.* **20**, 69–82 (2007).
- X. Xie and M. Mirmehdi, "MAC: magnetostatic active contour model," *IEEE Trans. Pattern Anal. Mach. Intell.* **30**, 632–646 (2008).
- X. Xie and M. Mirmehdi, "RAGS: region-aided geometric snake," *IEEE Trans. Image Process.* **13**, 640–652 (2004).
- L. Cohen, "On active contour models and balloons," *CVGIP: Image Understanding* **53**, 211–218 (1991).
- L. D. Cohen and I. Cohen, "Finite-element methods for active contour models and balloons for 2-D and 3-D images," *IEEE Trans. Pattern Anal. Mach. Intell.* **15**, 1131–1147 (1993).
- J. Cheng and S. Foo, "Dynamic directional gradient vector flow for snakes," *IEEE Trans. Image Process.* **15**, 1563–1571 (2006).
- J. Tang, "A multi-direction GVF snake for the segmentation of skin cancer images," *Pattern Recogn.* **42**, 1172–1179 (2009).
- A. Kovacs and T. Sziranyi, "Harris function based active contour external force for image segmentation," *Pattern Recogn. Lett.* **33**, 1180–1187 (2012).
- J. F. Ning, C. K. Wu, S. G. Liu, and S. Q. Yang, "NGVF: an improved external force field for active contour model," *Pattern Recogn. Lett.* **28**, 58–63 (2007).
- Y. Wang, Y. Jia, and L. Liu, "Harmonic gradient vector flow external force for snake model," *Electron. Lett.* **44**, 105–106 (2008).
- Z. Hou and C. Han, "Force field analysis snake: an improved parametric active contour model," *Pattern Recogn. Lett.* **26**, 513–526 (2005).
- K. He, J. Sun, and X. Tang, "Guided image filtering," in *Computer Vision-ECCV 2010* (Springer, 2010), pp. 1–14.
- C. Tomasi and R. Manduchi, "Bilateral filtering for gray and color images," in *Sixth International Conference on Computer Vision* (1998), pp. 839–846.